Schmidt and Housen [4] was then used to estimate transient-cavity diameters for a range of projectile sizes. Since the melt volumes are originally expressed in terms of impactor volume, it is a simple matter to relate the volume of impact melt to the dimensions of the transient cavity as given by the scaling relationship [4]. Three such curves are also included in Fig. 2. It is immediately apparent that the theoretical curves overestimate the quantity of melt by, in some cases, more than an order of magnitude. We believe that this reflects an underestimate of the transient-cavity dimensions rather than an overestimate of melt production for the following reasons: (1) The scaling relationship used for cavity dimensions was formulated partly on the basis of the *final* dimensions of craters formed in sand, which almost certainly represent adjusted transient cavities. (2) The melt-volume estimates are accurate to within a factor of 2, with underestimates being equally likely as overestimates, and thus cannot account for the differences. (3) Melt ejection could account for removal of up to 50% of the total produced at the smallest craters, but will have a vanishingly small effect in the cases of the largest craters in the figure. (4) The melt volumes calculated here, as evidenced by Fig. 1, are in good agreement with those determined from the more complex models. Lacking a detailed physical basis for changing the scaling relationship—which, it must be emphasized, combines with the melt calculations to yield a slope that is statistically indistinguishable from that of the terrestrial data—the model curve is brought into agreement with the terrestrial data simply by multiplying the model relationship for 25 km s^{-1} (the rms terrestrial impact velocity [12]) by a constant. The resulting relationship is

$$D_{tc} = 1.39\left(\frac{\rho_p}{\rho_t}\right)^{\frac{1}{3}} D_p^{0.78} V_i^{0.43} g^{-0.22} \quad (1)$$

where D_{tc} is the transient-cavity diameters, ρ_p and ρ_t are the projectile and target densities respectively, V_i is the impact velocity, and g is the gravitational acceleration, all in cgs units.

Final Crater Dimensions: Equation (1) can be written for final crater dimensions by direct incorporation of Croft's [11] modification scaling relationship, which can be written as

$$D_R \approx D_Q^{-0.18} D_{tc}^{1.18} \quad (2)$$

in which D_R is the final rim-crest diameter and D_Q is the diameter of the simple-to-complex transition for the planet (and terrain) in question. Substitution for D_{tc} into equation (1) and solving for D_R yields an equation of the form

$$D_R = k\left(\frac{\rho_p}{\rho_t}\right)^{0.39} D_p^{0.92} V_i^{0.51} \quad (3)$$

where k is a constant related to g and the value of D_Q. Values for D_Q and k are given in Table 2. Relationships described by equations (1) and (3) are used elsewhere in this volume in relating model melt volumes to observed characteristics of the terrestrial and planetary impact record, and in deriving certain implications of those relationships for the cratering record.

References: [1] O'Keefe J. D. and Ahrens T. J. (1977) *Proc. LSC 8th*, 3357. [2] Orphal D. L. et al. (1980) *Proc. LPSC 11th*, 2309. [3] Cintala M. J. (1992) *JGR, 97*, 947. [4] Schmidt R. M. and Housen K. L. (1987) *Int. J. Impact Eng., 5*, 543. [5] Grieve R. A. F. and Cintala M. J. (1992) *Meteoritics*, submitted. [6] Gault D. E. and Heitowit E. D. (1963) *Proc. 6th Hypervel. Impact Symp.*, 419. [7] Charters A. C. and Summers J. L. (1959) *NOLR 1238*, U.S. Naval Ordnance Laboratory, 200. [8] Thomsen J. M. et al. (1980) *Proc. LPSC 10th*, 2741. [9] Kieffer S. W. and Simonds C. H. (1980) *Rev. Geophys. Space Phys., 18*, 143. [10] Grieve R. A. F. et al. (1991) *JGR, 96*, 753. [11] Croft S. K. (1985) *Proc. LPSC 15th*, 828. [12] Shoemaker E. M. (1977) In *Impact and Explosion Cratering* (D. J. Roddy et al., eds.), 617, Pergamon, New York.

TABLE 2. Planet-specific constants for use in equation (3).

Planet	D_Q (km)	k ($cm^{-0.43}$ $s^{0.51}$)
Mercury	10.0	2.61×10^{-2}
Venus	4.0 (assumed)	2.54×10^{-2}
Earth	4.0	2.24×10^{-2}
Moon	10.9	3.38×10^{-2}
Mars	3.1	3.39×10^{-2}

514-90 11 N93-10126 475160

MELT PRODUCTION IN LARGE-SCALE IMPACT EVENTS: PLANETARY OBSERVATIONS AND IMPLICATIONS.

Mark J. Cintala[1] and Richard A. F. Grieve[2], [1]Code SN4, NASA Johnson Space Center, Houston TX 77058, USA, [2]Geophysics Division, Geological Survey of Canada, Ottawa, Ontario K1A 0Y3, Canada.

ND18500 GW970643

Differences in scaling relationships for crater formation and the generation of impact melt should lead to a variety of observable features and phenomena. These relationships infer that the volume of the transient cavity (and final crater) relative to the volume of impact melt (and the depth to which melting occurs) decreases as the effects of gravity and impact velocity increase. Since planetary gravity and impact velocity (Table 1) are variables in the calculation of cavity and impact-melt volumes [1], the implications of the model calculation will vary between planetary bodies; this contribution will address some of those differences. Details of the model calculations of impact-melt generation as a function of impact and target physical conditions have been provided elsewhere [1], as have attempts to validate the model through ground-truth data on melt volumes, shock attenuation, and morphology from terrestrial impact craters [2,3].

Melt Volumes: The volume of impact melt as a function of rim-crest diameter is shown in Fig. 1 for typical impact velocities at the five terrestrial planets [4] (Table 1). In the calculation of rim-crest diameter, a modified version of Schmidt and Housen [5] scaling was used to calculate transient-cavity diameters [3], which were converted to final rim-crest diameters using the "modification scaling" relation of Croft [6]. Chondritic projectiles were used in all calculations, and assumed target materials varied by planet (Table 1). Figure 1 indicates that relative melt volumes at craters of a given

TABLE 1. Variables used in the calculations of impact melting and crater dimensions. All targets were assumed to have a temperature of 273 K except for Venus, for which 700 K was used.

Planet	Target	V_i (km s^{-1})	Gravitational Acceleration (cm s^{-2})
Mercury	Anorthosite	23.6	370
Venus	Diabase	19.3	891
Earth	Granite	17.8	981
Moon	Anorthosite	14.1	162
Mars	Anorthosite	12.4	371

size increase in the order Moon, Mars, Mercury, Earth, and Venus; for the purpose of illustration, we concentrate here on the endmember cases, Venus and the Moon. For example, an impact event creating a 100-km crater on the Moon also results in about 1200 km³ of impact melt, compared to about 3500 km³ in a comparably sized crater on Venus. Because the bulk of the impact melt inside large, complex craters in crystalline targets occurs as coherent melt sheets, this disparity means that features such as visible central structures and floor roughness, which reflect parautochthonous target material of the true crater floor and walls, will be less buried by melt and most prominent in lunar craters compared to craters on the other terrestrial planets.

It has become something of a tenet that the depth of craters and the diameters at which they undergo morphological transitions are inverse functions of planetary gravity [7,8]. Although there is a general progression toward increasing depth with decreasing gravity, the data show considerable variance and the inverse relationship is not strict [9]. The effects of gravity in determining crater depth are generally assumed to be in limiting and maintaining topography during and after cavity modification [8]. This work indicates another potential role for gravity through its effect on relative impact-melt volumes. If rectangular cross sections were assumed, for instance, our standard 100-km lunar crater would have an interior melt sheet about 125 m thick, compared to one about 450 m thick for its venusian counterpart. This disparity is a minimum, as the lower lunar gravity will favor relatively more ejection of melt. Current estimates of the ratio of the apparent depth/diameter relationships [7,10] for complex craters on the Moon and Venus are between 4 and 6, compared to a 1/g ratio for the two planets of 5.5. Taking the melt volumes into account and calculating true depths (i.e., depth to the true crater floor) gives a ratio of true depth/diameter of ~2.5–3. This suggests that the called-for 1/g relation for apparent depths may be fortuitous and that gravity and other planet-specific properties (such as impact velocity and physical properties of the target, including the presence of volatiles on planets such as Mars), might play a complex and sometimes competing role.

Crater and Basin Morphology: Previously, we have suggested that the increased depth of melting with increasing crater size will result in weakening of the base of the transient cavity [2,3]. On

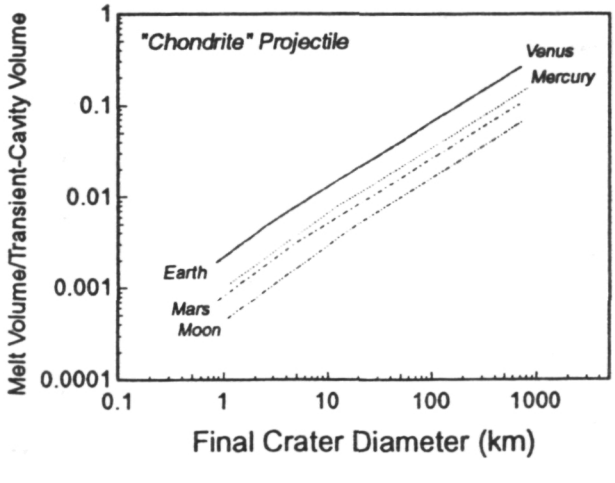

Fig. 1. Volume of impact melt relative to that of the transient cavity as a function of final crater diameter. Generated for the conditions listed in Table 1, a separated curve is presented for each planet.

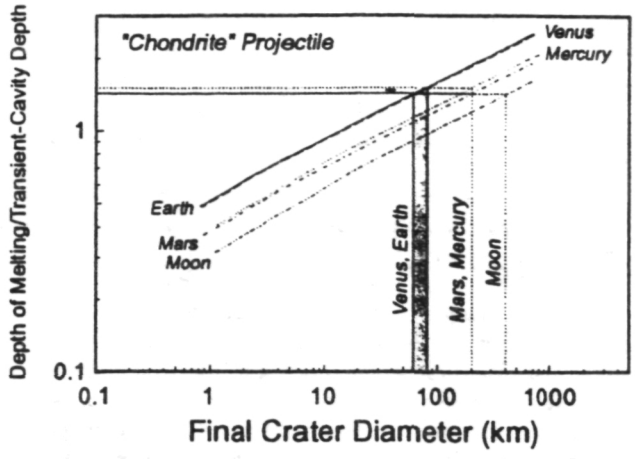

Fig. 2. Depth of melting relative to the transient cavity's depth as a function of final crater diameter. Similar values appear on the vertical axis for the diameters at which maxima occur in the frequency of peak-ring basins.

cavity modification and uplift, this material will be unable to form a coherent central peak. The zone of melting will approach and ultimately intersect the base of the transient cavity (Fig. 2), at which point the base of the cavity will have no strength. The only possible central topographic form in such a case is an interior ring. When the diameter at which maximum development of peak rings in craters on the terrestrial planets is considered, and the corresponding relative depths of melting are determined, they define a very restricted set of melting depths (Fig. 2). While we will not defend these actual values, we do suggest that the small range over which they occur (Fig. 2) could be considered as a validation of the general concept that impact melt could have a role in peak-ring formation. While one could argue that this could also be fortuitous, we note the additional prediction of this model that, as crater diameter increases and progressively more of the transient-cavity floor is melted, the diameter of the inner (peak) ring will increase. Although not emphasized in the literature, this has been noted for a relatively small set of 12 lunar basins, where the peak-ring diameter/rim-crest diameter ranges from 0.45 to 0.56, and is generally inversely correlated with size [11]. This change in relative ring diameter with size, from 0.28 to 0.67 [12], is more obvious from a larger mercurian dataset of 45 craters. It has most recently been shown to occur on the basis of 16 venusian craters [13] changing from 0.29 to 0.67, with even smaller ratios occurring at the transition from central peak to peak-ring craters.

We offer the impact-melting mechanism of peak-ring formation as an alternative, at least supplemental, explanation to the previous hypothesis that invoked the collapse of overheightened central peaks [14]. Even if it accounts for the formation of rings, this latter hypothesis does not specifically allow for the disappearance of central peaks with increasing crater size. The model here also maintains functionality with variations in planetary gravity through the scaling of crater dimensions. While at first glance it might seem to be at variance with other mechanisms suggested for ring formation [15], it is an alternative method of reducing rock strength in and around the transient cavity, as required in some of those models. In addition, wholesale, deep-seated melting in truly large basin-forming events will result in inward flow during modification, possibly leading to circumferential faulting and outer-ring formation. Thus,

it might reduce the need for such weakening mechanisms as acoustic fluidization [16], and might provide a substitute for the "asthenospheric" flow required in these models of basin-forming events.

A few central uplifted structures in complex craters are acentrally located, which has been ascribed to preimpact structural control [17]. Oblique impact, however, can produce asymmetric melt zones, with increased melting in the direction of impact [18]. Thus, asymmetric impact melting followed by uplift may be an alternative mechanism of formation of acentral peaks.

Impact Lithologies: There will be second-order differences in the impact lithologies at comparable-sized craters on the terrestrial planets because of the effect of gravity on scaling relations. For example, the levels of recorded shock in uplifted central structures and the ratio between melted and clastic material will be lower in lunar craters than in those on other terrestrial planets, other parameters being equal. These potential differences must be considered when interpreting remote-sensing data [19]. Similarly, the various proportions of impact lithologies and their second-order characteristics will vary with the size of the event. At larger impact events, for instance, there will be less clastic debris available within the transient cavity for incorporation into the melt. Such implications of differential melting and cratering have been used to explain some of the observations at large terrestrial impact melt sheets such as at Sudbury [20]. Similar arguments apply to lunar samples. The lack of clasts is therefore an insufficient single condition to rule out an impact-melt origin for relatively coarse-grained, igneous-textured rocks in the samples from the lunar highlands.

References: [1] Cintala M. J. (1992) *JGR, 97*, 947. [2] Grieve R. A. F. and Cintala M. J., this volume. [3] Grieve R. A. F. and Cintala M. J. (1992) *Meteoritics*, submitted. [4] Strom R. G. and Neukum G. (1988) In *Mercury* (F. Vilas et al., eds.), 336, Univ. Ariz., Tucson. [5] Schmidt R. M. and Housen K. L. (1987) *Int. J. Impact Eng., 5*, 543. [6] Croft S. K. (1985) *Proc. LPSC 15th*, 828. [7] Pike R. J. (1980) *Icarus, 43*, 1. [8] Melosh H. J. (1989) *Impact Cratering: A Geologic Process*, Oxford, 245 pp. [9] Cintala M. J. et al. (1977) *Proc. LPSC 8th*, 3409. [10] Garvin J. B. and Schaber G. G. (1992) *LPSC XXIII*, 399. [11] Head J. W. (1977) In *Impact and Explosion Cratering* (D. J. Roddy et al., eds.), 563, Pergamon, New York. [12] McKinnon W. B. (1981) In *Multi-Ring Basins*, 259, Pergamon, New York. [13] Alexopoulos J. S. and McKinnon W. B. (1981) *JGR*, in press. [14] Grieve R. A. F. et al. (1981) In *Multi-Ring Basins*, 37, Pergamon, New York. [15] Melosh H. J. (1982) *JGR, 87*, 371. [16] Melosh H. J. (1979) *JGR, 87*, 7513. [17] Schultz P. H. (1972) *Moon Morphology*, Univ. Texas, Austin, 626 pp. [18] O'Keefe J. D. and Ahrens T. J. (1986) *Science, 234*, 346. [19] Pieters C. M. (1982) *Science, 215*, 59. [20] Grieve R. A. F. et al. (1991) *JGR, 96*, 753.

STRUCTURAL REVIEW OF THE VREDEFORT DOME.

W. P. Colliston[1] and W. U. Reimold[2], [1]Department of Geology, University of the Orange Free State, P.O. Box 339, Bloomfontein 9300, South Africa, [2]Economic Geology Research Unit at the Department of Geology, University of the Witwatersrand, P.O. Wits 2050, Johannesburg, South Africa.

The structure of the older-than-3.2-Ga Archean basement and Archean-to-Precambrian sedimentary/volcanic rocks (3.07 to ca. 2.2 Ga) in the center of the Witwatersrand Basin to the southwest of Johannesburg (South Africa) is dominated by the ca. 2.0-Ga megascopic Vredefort "Dome" structure.

The effect of the "Vredefort event" is demonstrably large and is evident within a northerly arc of about 100 km radius around the granitic core of the structure. Northerly asymmetric overturning of the strata is observed within the first 17 km (strata is horizontal in the south), followed by a 40-km-wide rim synclinorium. Fold and fault structures (normal, reverse, and strike-slip) are locally as well as regionally concentrically arranged with respect to the northern and western sides of the structure.

The unusual category of brittle deformation, the so-called "shock deformation," observed in the collar strata has attracted worldwide attention over the past two decades. These deformation phenomena include the presence of coesite and stishovite, mylonites and pseudotachylites, cataclasis at a microscopic scale, and the ubiquitous development of multiply striated joint surfaces (which include "shatter cones," orthogonal, curviplanar, and conjugate fractures).

The macroscopic to microscopic deformation features have led to the formulation of various hypotheses to account for the origin of the Vredefort structure: (1) tectonic hypotheses: deep crustal shear model [1], doming and N-directed thrust fault model [2], fold interference model [3], and diapir model [4]; (2) the exogenous bolide impact hypothesis [e.g., 5,6]; and (3) the endogenous cryptoexplosion model [7].

Ongoing structural studies on the dome [8] have aided in narrowing the field of possible hypotheses. The subvertical faults and shears associated with diapirs or an endogenic cryptoexplosion could not be identified in either the basement or the collar rocks. The subvertical conjugate northwest- and northeast-trending shear zones that occur in the migmatitic basement predate the extrusion of the ca. 3.07-Ga-old Dominion Group volcanics. Toward the southern extremity of the structure, subhorizontal gneissic fabrics, which are deformed by the subvertical shears, become more prominent. The majority of the macrostructural deformation (faulting, folding) in the collar is related to the Vredefort event, and the remainder to reactivation of pre-Vredefort structures. Pseudotachylite occurrence is not exclusive to the Vredefort structure and is found throughout the northern and northwestern Witwatersrand Basin. Several pseudotachylite generations were produced over a wide interval from 2.2 to 1.1 Ga (pre- to post-Vredefort event) [9]. This suggests the regional occurrence of episodic brittle deformation events with associated high-strain intensities.

It has been identified that the multiply striated joint surfaces postdate the overturning and related faulting in the structure, as well as a phase of postoverturning pseudotachylite development. These observations do not conform to the generalizations proposed by other workers who assume a horizontal stratigraphy prior to shatter cone development by an impact-generated shock wave [e.g., 10,11]. It also places doubt on the validity of using shatter cones as a diagnostic criterion for impact structures. Although the presence of coesite and stishovite cannot yet be fully explained, it is suggested that these high-pressure polymorphs and multiply striated joint surfaces may also be produced in a tectonic regime by Mohr-Coulomb fracture within varying local stress fields.

According to regional gravity and aeromagnetic data the domal structure is interpreted to be located at the intersection of a northwest-trending anticlinal arch (which uplifts lower crust) and a north/northwest-axis of crustal downwarp (corresponding to the long axis of the Witwatersrand Basin) [12]. Reflection seismic data along a line roughly parallel to the northwest-anticlinal arch confirms regional structural data and interpretations of the structure [13,1]: The deep structure in the basement reveals only subhorizontal reflectors, which undergo a change in dip (overturned with the collar